IEEE Access
Multidisciplinary ⋮ Rapid Review ⋮ Open Access Journal

Received February 2, 2022, accepted February 27, 2022, date of publication March 2, 2022, date of current version March 11, 2022.

Digital Object Identifier 10.1109/ACCESS.2022.3155776

Efficient Protocol to Use FMCW Radar and CNN to Distinguish Micro-Doppler Signatures of Multiple Drones and Birds

SEWON YOON[1], SOOBUM KIM[2], JOOHO JUNG[3], SANGBIN CHA[1], YOUNGSEOK BAEK[5], BONTAE KOO[5], INOH CHOI[6], AND SANGHONG PARK[1]

[1]Department of Intelligent Robot Engineering, Pukyong National University, Busan 48513, Republic of Korea
[2]Radsys, Daegu 42918, Republic of Korea
[3]Electromagnetic Technology Research Center, Kookmin University, Seoul 02707, Republic of Korea
[4]Department of Electronics Engineering, Pukyong National University, Busan 48513, Republic of Korea
[5]Electronics and Telecommunications Research Institute, Daejeon 34129, Republic of Korea
[6]Department of Electronics and Communications Engineering, Korea Maritime & Ocean University, Busan 49112, Republic of Korea

Corresponding author: Sanghong Park (radar@pknu.ac.kr)

This work was supported in part by the Basic Science Research Program through the National Research Foundation of Korea (NRF) funded by the Ministry of Science, Information and Communication Technologies, and Future Planning under Grant 2018R1D1A1B07044981, in part by the Institute of Information and Communications Technology Planning and Evaluation (IITP) grant funded by the Korea Government (MSIT) for Development of Ultra-Low Power Intelligent Edge SoC Technology Based on Lightweight RISC-V Processor under Grant 2018-0-00197, and in part by NRF under project BK21 FOUR (Smart Robot Convergence and Application Education Research Center).

ABSTRACT Classification of multiple drones and birds by comparing micro-Doppler (MD) signatures is a very difficult task because the MD signatures of multiple birds can contaminate the MD signature of drones, and because a single drone can yield a very similar MD signature to that of multiple drones. In this paper, assuming a real observation scenario, we propose three protocols and analyze their accuracy in classification of multiple drones and birds by using the frequency modulated continuous wave radar and a convolutional neural network classifier. In simulations using models of rotating blades and of flapping wings, the method that uses training data that include combinations of drone and bird achieved an accuracy $\sim$ 100 % for the majority vote classification; this result demonstrates that ours is the most appropriate method to distinguish multiple drones from birds.

INDEX TERMS Aerial drones, rotating blade model, micro-Doppler, CNN, FMCW radar.

I. INTRODUCTION

Aerial drones are widely used for in many purposes such as military reconnaissance, aerial mapping, and environmental monitoring. However, they have been used for illegal surveillance of private land and military facilities. Therefore, efficient methods are required to detect drones and distinguish them from similar targets, mainly birds. Drones and birds can be classified by automatic target recognition techniques that use radar. High resolution range profiles (HRRPs) and inverse synthetic aperture radar (ISAR) images [1]–[3] are not effective for this task, because birds have similar sizes and radar cross sections (RCSs) ($\sim$20 dBsm) as drones.

Micro-Doppler (MD) is the time-varying Doppler frequency caused by the time-varying micro-motion of a target [4]–[8] such as rapid rotation and vibration. A drone blade is engaged in fast 2D rotation so its MD in the time-frequency (TF) domain is symmetric [5], [6] and the bandwidth is large, whereas the MD of a bird is caused by slow wing flapping, which is not symmetric, and the bandwidth is small. Therefore, difference in micro-motion can be very effective to distinguish drones from birds, despite their similar RCSs.

Several methods to classify drones by using MD images (MDIs) in the TF domain have been proposed [9]–[14]. Most of them extract distinctive features from the MDI in the TF domain, then apply them to a well-designed classifier, or use MDI itself in classifiers that use neural networks. One method [9] uses a modified adaptive boosting algorithm to classify rotating targets, and two recently-proposed methods [10], [11] propose efficient features in the time-velocity diagram of the drone and the bird MD, then apply the developed features to a well-designed boosting classifier. Other methods use the MDI and cepstrograms for classification [12], or propose some good features to classify drones [13], or use a convolution neural network (CNN) with merged Doppler images to classify drones [14].

The associate editor coordinating the review of this manuscript and approving it for publication was Weimin Huang.

Existing methods use MDIs obtained from a single drone and a single bird; these MDIs and their features differ greatly between these two groups, so high classification results ∼100% are achieved by using simple features and classifiers. However, in real observation scenarios, numerous drones and birds may fly with similar motion parameters and generally occur in a single radar beam. In this case, MDIs are totally different; range profiles (RPs) of each target overlap and sum to yield MDIs that differ from those of the single target, so the classification task becomes extremely difficult. Therefore, the solution to this problem requires an efficient protocol that can improve the classification accuracy, rather than an improved classifier. To the best of our knowledge, no papers have suggested efficient methods for simultaneous classification of multiple targets.

Here, we suggest three classification protocols that each use a CNN classifier, and that can be used as a reference for multiple drone-bird recognition and be further improved for other multiple-target recognitions. Then we analyze the advantages and weaknesses of each method in various classification scenarios, and identify the most adequate protocol. Protocols are as follows:

1) In the first protocol, the training database (TR) is constructed using MDIs of a single drone and a single bird, assuming that targets are separated in the range domain using RPs. High resolution methods such as the multiple signal classification (MUSIC) [15] and relaxation (RELAX) [16] algorithms are applied to improve the range resolution, and the Zao-Atlas-Marks (ZAM) [17] method is applied to achieve high resolution in the TF domain.
2) In the Second protocol, the TR is constructed using MDIs of a single drone and a single bird, and MDIs obtained by the random combination (MDIR) of single drone and the single bird are added.
3) The third protocol is to construct a TR obtained by MDIs of a drone, a drone + a bird, a drone + two birds, two drones, two drones + a bird, two drones + two birds, a bird, and two birds.

The remainder of our paper is organized as follows: Section II introduces the radar signal model, the principle of MD imaging, the construction of TRs, and the general procedure for classification using CNN. Section III describes three proposed protocols for multi-target recognition. Section IV analyzes and compares the accuracy of each protocol for various observation scenarios and finally, Section V presents our conclusions for the classification of the multiple drones and birds.

II. MATHEMATICAL MODELING AND CLASSIFICATION PROCEDURE

A. MATHEMATICAL MODELING OF DRONE BLADE AND BIRD WING

We used a signal model described previously [18], and assumed that the drone is a quadcopter, which is the most widely used type. The quadcopter has four rotors and each

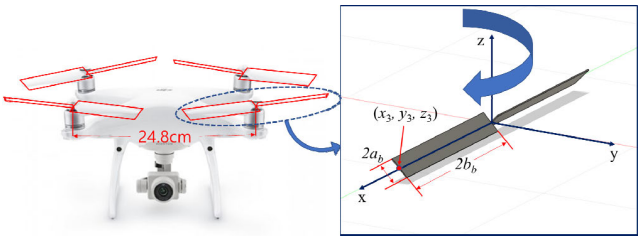

FIGURE 1. Quadcopter model and blade rotation.

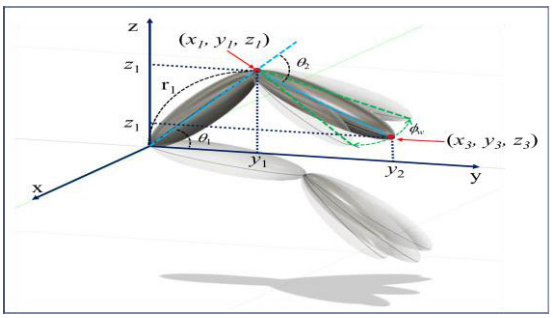

FIGURE 2. Geometry of the bird micro-motion.

rotor has two blades that have dimensions $2a_b \times 2b_b$ ($a_b < b_b$) that are 180° apart and rotate around the rotor axis at rotation frequency f_b (Fig. 1). In modeling the MD signal of the blade, the two blades were placed along the x axis and each blade was twisted by 45° around the x axis, in opposite directions. The blades were rotated around the z axis clockwise in a local coordinate (Fig. 1) and shifted by the center $\mathbf{o}_p$ of the rotor p ($p = 1$, 2, 3, or 4). The coordinate of the blade q is given by

$$\mathbf{r}_q(t)\begin{bmatrix} x_q \\ y_q \\ z_q \end{bmatrix} = \mathbf{R}(t)\mathbf{b}_q = \begin{bmatrix} \cos(2\pi f_b t) & \sin(2\pi f_b t) & 0 \\ -\sin(2\pi f_b t) & \cos(2\pi f_b t) & 0 \\ 0 & 0 & 1 \end{bmatrix}\mathbf{b}_q, \tag{1}$$

where blade index q = (1 or 2), and $\mathbf{b}_q$ is the initial coordinate of blade q; $\mathbf{b}_1 = [-2b_b\ 0\ 0]^{\mathrm{T}}$ and $b_2 = [-2b_b\ 0\ 0]^{\mathrm{T}}$. Then position $\mathbf{o}_{p,q}$ of the blade q at rotor p is given by

$$\mathbf{o}_{p,q} = \mathbf{r}_q + \mathbf{o}_p. \tag{2}$$

Assuming a plate that is observed at a line-of-sight vector line-of-sight (LOS) composed of an azimuth angle ϕ and an elevation θ, the RCS of the flat plate twisted by 45° is [19]

$$\mathrm{RCS} = \left(\cos\theta \frac{\sin x'}{x'} \frac{\sin y'}{y'}\right), \tag{3}$$

where

$$x'(2\pi/\lambda)a_b \sin\theta \sin\phi, \quad y' = (2\pi/\lambda)b_b. \tag{4}$$

Using the same $\mathbf{R}(t)$ in (1), RCS of each blade is obtained at each LOS by using (2).

The bird motion was modeled by considering the pectoralis major ('lower') and supracoracoideus ('upper') muscles (Fig. 2). With the same sinusoidal frequency f_w, we assumed that the lower muscle tip at (x_1, y_1, z_1) rotated by $\theta_1 = 40° \cos(2\pi f_w t) + 15°$ and the upper muscle tip at (x_2, y_2, z_2) rotated by $\theta_2 = 30° \cos(2\pi f_w t) + 40°$. The forward-backward movement of the upper wing was modeled by rotating (x_2, y_2, z_2) by $\phi_w = 20° \cos(2\pi f_w t) + 40°$ in the x-y plane. As a result, the lower muscle position $\mathbf{w}_1$ and upper muscle position $\mathbf{w}_2$ are

$$\mathbf{w}_1 = \begin{bmatrix} 0 \\ r_1 \cos\theta_1 \\ y_1 \tan\theta_1 \end{bmatrix},$$
$$\mathbf{w}_2 = \begin{bmatrix} r_2 \tan\phi_w \\ y_1 + r_2 \cos\phi_w \cos(\theta_1 - \theta_2) \\ z_1 + (y_2 - y_1)\tan(\theta_1 - \theta_2) \end{bmatrix}, \quad (5)$$

where

$$r_1 = \sqrt{x_1^2 + y_1^2 + z_1^2}$$
$$r_2 = \sqrt{(x_2 - x_1)^2 + (y_2 - y_1)^2 + (z_2 - z_1)^2} \quad (6)$$

As in (2), (5) is shifted by the center of the bird $\mathbf{u}_c$ to model the total MD so the position $\mathbf{g}_a$ of each muscle is

$$\mathbf{g}_a = \mathbf{w}_a + \mathbf{u}_c, \quad (7)$$

where a is 1 (= lower muscle) or 2 (= upper muscle).

Modeling the RCS of the wing muscle is extremely difficult because the wing muscle is different depending on bird types and the material of the muscle; in this paper, the muscle was approximately modeled by the ellipsoid whose RCS is given analytically. RCS of the ellipsoid observed at an observation angle θ with respect to the major axis is given by

$$\text{RCS} = \frac{\pi (a_w/2)^4 (b_w/2)^2}{((q_w/2 \times \sin\theta)^2 + (b_w/2 \times \cos\theta)^2)^2}, \quad (8)$$

where a_w and b_w are the lengths of the minor and the major axes, respectively [19]. For the lower muscle, θ is the angle between LOS and $\mathbf{w}_1$, and for the upper muscle, θ is the angle between LOS and ($\mathbf{w}_2$ - $\mathbf{w}_1$).

B. RADAR SIGNAL MODELING FOR MD

We used an FMCW radar signal model described previously [18]. A FMCW radar continuously transmits and receives a chirp signal that has a period T_{chirp} The transmitted chirp signal is given by

$$s_T(t) = \exp\left(j2\pi(f_0 t + \frac{K_r t^2}{2})\right), \quad (9)$$

where f_0 is the minimum frequency, $K_r = BT_{chirp}$ is the chirp rate. The received chirp from a scatterer at r is given by

$$s_R(t) = \exp\left(j2\pi(f_0(t-\tau) + \frac{K, (t-\tau)^2}{2})\right), \quad (10)$$

where the time delay $\tau = 2r/c$ and c is the speed of the light.

After dechirping the received chirp by the transmitted chirp, the intermediate signal $s_{IF}(t)$ is yielded as

$$s_{IF}(t) = \exp\left(j2\pi(f_0\tau + K_r\tau t - \frac{K_r\tau^2}{2})\right), \quad (11)$$

where $K_r\tau$ is the beat frequency and is related to r as:

$$f_b = K_r\tau = \frac{2K_r}{c} r. \quad (12)$$

The third term $K_r\tau^2/2$ is the residual video phase and is removed.

When a blade or a bird muscle with an RCS A_0 is observed at every slow-time $t_s = kT_{chirp}$ during a coherent processing interval T_{CPI}, the received signal is given by

$$s_0(t, t_s) = A_0 \exp\left\{-j\frac{4\pi f_0 R(t_s)}{c}\right\} \times \exp\left(j\pi K_r\left(t - \frac{2R(t_s)}{c}\right)^2\right), \quad (13)$$

where $R(t_s)$ is the distance to the target at t_s. Then the dechirped signal $s_{0d}(t, t_s)$ is given by

$$s_0(t, t_s) = A_0 \exp\left\{-j\frac{4\pi f_0 R(t_s)}{c}\right\} \times \exp\left(j2\pi\left(f_c\tau + K_r\tau t - \frac{1}{2}K_r\tau^2\right)\right). \quad (14)$$

Removing $\exp(-j\pi K_r\tau^2)$ and Fourier-transforming (FT) in the t domain to the frequency f-domain yield RPs $s_r(f, t_s)$ at t_s as

$$s_r(f, t_s) = A_0 \exp\left\{-j\frac{4\pi(f_0 + f)}{c} R(t_s)\right\} p_r(f - K_r\tau), \quad (15)$$

where $p_r(\cdot)$ is a sinc function formed by the rectangular window with a length T_{chirp}.

When a target in a range bin is engaged in micro-motion, the signal in this bin is time-varying and sampled with an interval t_s. Therefore, the signal $s_{MD}(t_s) = s_r(f_{bt}, t_s)$, where f_{bt} is the beat frequency of the target at r, can be used to analyze MD. Because of the time-varying nature of MD, it is more desirable to analyze it in TF domain. In this paper, we use the short-time Fourier transform (STFT) which is the successive FT of signals in the window $W(\zeta)$ shifted by t_s STFT of $s_{MD}(t_s)$ is given by

$$MD(t_s, f_s) = \int_{-\infty}^{\infty} S_{MD}(\zeta) W^*(\zeta - t_s) e^{-j2\pi f_s \zeta} d\zeta, \quad (16)$$

where f_s is the MD frequency [20]. To analyze the improvement in the resolution, we also applied the ZAM method, which removes the cross-term interference by using a well-designed kernel function.

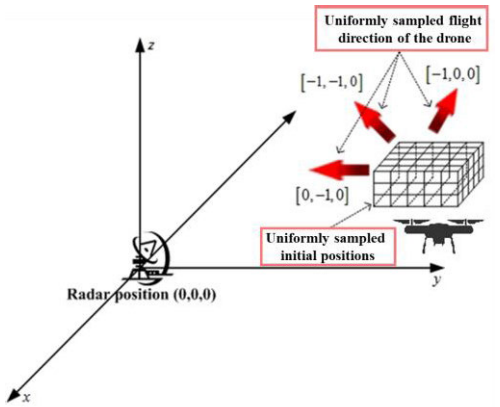

FIGURE 3. Method to construct the TR.

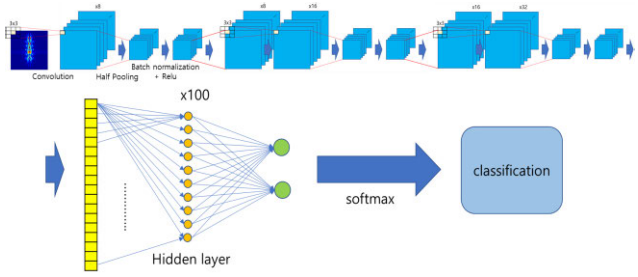

FIGURE 4. CNN classifier.

C. CONSTRUCTION OF TR, CNN, AND OVERALL PROCEDURE

In this subsection, we explain TR, CNN, and the overall procedure for singletarget classification using a single TFI because they guarantee high P_c once targets are completely separated. Those of multiple targets using multi-aspect TFIs in each protocol are explained introduced in section III.

The TR for classification should be constructed for all cases; i.e., all combinations of aspect angles, directions of flight, and frequencies of blade rotation and wing flapping This computation requires huge time and memory space, so we constructed the TR for the single target classification by considering the flight scenario (Fig. 3) [7]; we sampled the 3D training space with a uniform interval and flew the target in a given direction at each given grid point.

To consider the variation of flight direction and MD frequency, the flight direction was also sampled between $\pm\theta_t$ in increments $\Delta\theta_t$, and f_b of the drone blade was sampled between $f_{b,1}$ and $f_{b,2}$ in increments Δf_b, and f_w of the bird wing was sampled between $f_{w,1}$ and $f_{w,2}$ in increments Δf_w. Finally, MDIs were obtained for all combinations of aspect angles, flight directions, and motion parameters. In addition, to remove the time-domain variance of the MDI, the cadence velocity diagram (CVD) which is FT of the MDI in time-domain, was used for classification.

The classifier used in this paper is a CNN (Fig. 4), which is applied for many purposes due to its excellent classification

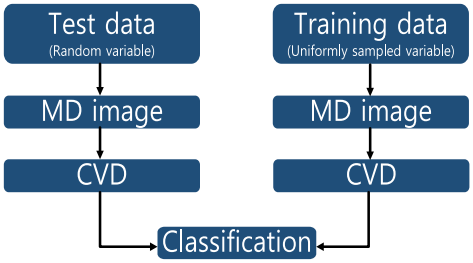

FIGURE 5. Classification procedure.

accuracy [14], [21]; compared with conventional methods that rely on the extracted features from the data, CNN can find features from data and decision boundaries while minimizing the cost function. Furthermore, in contrast to the extreme difficulty of the conventional methods in finding features for multiple target classification, a CNN can achieve high classification accuracy if an appropriate TR to explain multiple targets is provided. The cost function used for CNN is the average classification error

$$Cost_{tr} = \frac{1}{N_{tr}} \sum_{i=1}^{N_{tr}} \left| \hat{R}_i - R_i \right|, \tag{17}$$

where $\hat{R}_i$ is the output of CNN for the ith training image, and R_i is the true class of it (drone = '0' and bird = '1'). Many papers and books (e.g., [14], [21]) have described CNN structure and function, so the principle and details are omitted.

Classification was conducted following the general target-recognition procedure (Fig. 5). During the training phase, targets (Fig. 1 or 2) with the uniformly-sampled motion parameters (= direction, velocity, and micro-motion parameters) were placed on the uniform grids (Fig. 3) and the radar signal was constructed using (14) and (15). Then MDI was calculated by (16), and CVDs of MDIs were obtained by FT in the time domain, and CNN is trained using the obtained CVDs. Then the test MDIs and CVDs of randomly-selected numbers of drones were obtained by using randomly selected locations, flight directions, and motion parameters in the range of each parameter. Finally, classification was conducted by using the trained CNN classifier. The accuracy is represented by the correct-classification ratio

$$P_c = \frac{\text{No. of correct classifications}}{\text{No. of test images}}. \tag{18}$$

III. PROPOSED PROTOCOLS

A. FIRST PROTOCOL

The protocol proposed in this paper uses separation of targets in the range-domain (Fig. 6). In this protocol, peaks are found in the RP to extract MD signals of drones and birds, and MDIs are obtained using the clipped signal. Our main concern is to classify drones from birds, so the first classification is conducted to determine whether the MDI belongs to the drone or the bird. If the MDI is classified as a bird, the classification ends, but if it belongs to a drone, further classification

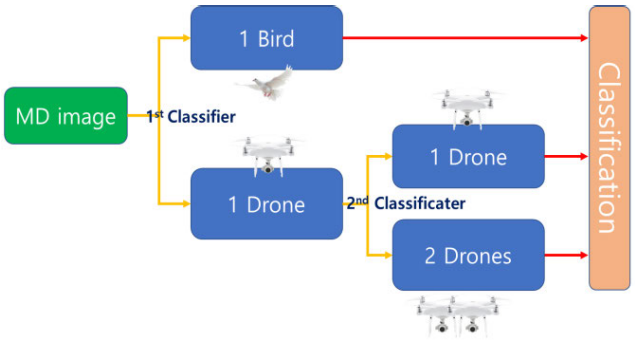

FIGURE 6. First protocol. Procedure is described in the text.

is conducted to determine whether the number of drones is 1 or 2.

The advantage of this protocol is that TR of the single target can be used for classification in the first step. Drones and birds have very different MD bandwidth and frequency, so the first classification is a very easy task that can be conducted with a small number of features or a simple CNN classifier. During the second classification, the effect of bird can be minimized because its MD is assumed to be separated in the first classification, and the single target TR can be used to determine whether the MD belongs to a single drone or two drones. However, construction of the TR for two drones in a range bin is a very difficult task, because drones can have different flight directions and motion parameters. Therefore, we construct the TR for two drones in a random manner; i.e., we select a random position, place two drones within a range resolution from the selected position, then store in the TR the MDIs of drones flying in random directions and motion parameters. A radar signal can contain >2 drones, but we did not consider that many, because simultaneous occurrence of these numbers of drones is very rare, and because P_c can degrade considerably due to the similar MDIs of multiple drones ≥2 (results shown in IV.*B*).

This protocol may yield classification errors once targets are not properly separated. If birds and drones occur simultaneously in a range bin, or if parts of bird and drones overlap with complete bodies of birds or drones, the MDIs can be seriously contaminated, so P_c can be considerably decreased due to MDIs being different from those in the TR. Considering all cases of overlaps is very difficult and uses enormous memory; therefore, separation of the targets before MD imaging is very important for classification. In this paper, we used three existing techniques to separate targets in the range domain.

The first technique is to zero-pad in the frequency domain. FT and inverse FT provide samples spaced at the inverse of the signal length, so zero-padding in the frequency domain of the RP can increase the number of range samples so targets are better separated.

The second technique is the MUSIC algorithm, which takes advantage of the fact that the direction vector $\mathbf{e}(r)$ at a range r is orthogonal to the noise subspace that consists of L noise eigenvectors $\mathbf{u}_1, \mathbf{u}_2, \ldots, \mathbf{u}_L$ [15]. The RP is given by

$$\mathbf{p}(r) = \frac{1}{\sum_{i=1}^{L} \left|\mathbf{u}_i^H \mathbf{e}(r)\right|^2}, \tag{19}$$

The third technique is to use the RELAX algorithm which is a nonlinear least squares relaxation algorithm to extract information such as the location and the amplitude of the scatterer by minimizing the cost function

$$\text{cost} = \left\| \mathbf{y} - \sum_{k=1}^{K} \mathbf{w}(f_k) a_k \right\|, \tag{20}$$

where K is the total number of the scatterers, $\mathbf{y}$ is the FT of the complex RP, f_k and a_k are the frequency and the amplitude of the scatterer k; f_k contains the information on the range of the scatter k. $\mathbf{w}$ is the FT vector that corresponds to f_k (details in [16]).

To further increase the resolution of TFI, we used the ZAM method which is a high-resolution TF transform method derived from the Wigner-Ville distribution [17], which is a transform that exploits autocorrelation and provides high resolution but suffers from cross-term interference. The ZAM method removes the cross-term experience by applying a well-designed kernel function $\Phi(\gamma, \tau)$ to the ambiguity function $\text{AF}(\gamma, \tau)$ of a signal $s(t)$ as follows [19]:

$$Z(t, \omega) = \int_{-\infty}^{\infty} \int_{-\infty}^{\infty} AF(\gamma, \tau) \Phi(\gamma, \tau) \times \exp\left(-j(\gamma t + \omega\tau)\right) d\tau d\gamma, \tag{21}$$

where

$$AF(\gamma, \tau) = \frac{1}{2\pi} \int_{-\infty}^{\infty} s(t + \frac{\tau}{2}) * s(t - \frac{\tau}{2}) e^{j\gamma t} dt, \tag{22}$$

$$\Phi(\gamma, \tau) = \frac{\sin(\pi\gamma\tau)}{\pi\gamma\tau} e^{-2\pi\alpha\tau^2}, \tag{23}$$

and * is the complex conjugate operator and α is a proper constant.

In addition, TFIs at various aspect angles are obtained in the real observation scenario, so we used the CNN classifier combined with the majority-vote rule; according to this rule, for the multiple classifications at various aspect angles, the class that has the most classification results is determined to be the class to which the test data belong. The final class C_F is determined as [22]

$$C_F = \underbrace{\max}_{k} N_k, \quad k = 1, \ldots, C_T, \quad N_T = \sum_{k=1}^{C_T} N_k, \tag{24}$$

where N_k is the number of cases determined to be the class k by CNN, and N_T is the total number of TFIs observed.

In this protocol, drones and birds are assumed to be completely classified, so TFIs in classifying the number of drones do not contain MD of birds. However, when birds fly very close to drones, the task of separating drones from birds is very difficult, so combinations of birds and drones should be considered. Drones and birds can be located at the same range bin with random flight directions and motion parameters, so the training data for this combination should be considered. The second protocol does this.

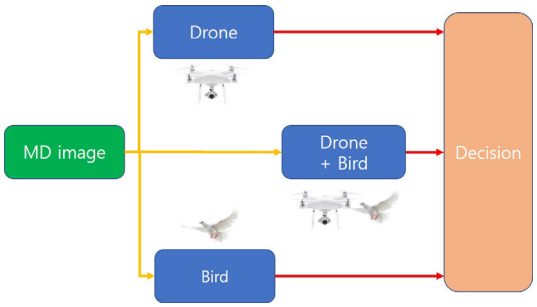

FIGURE 7. Second protocol Procedure is described in the text.

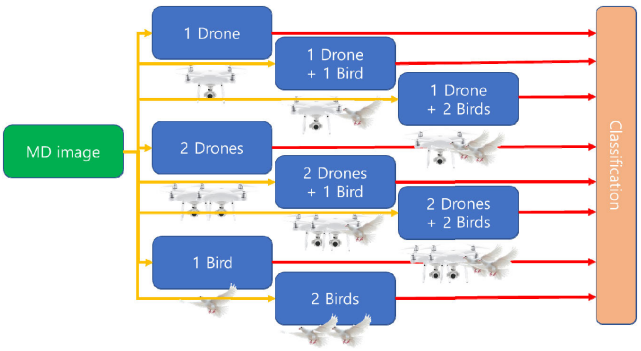

FIGURE 8. Third protocol. Procedure is described in the text.

B. SECOND PROTOCOL

The second protocol proposed in here still uses single-target recognition but considers combinations of a single target + a single bird (Fig. 7). The single-drone training data is constructed as in the second classification of the first protocol, by using the uniformly sampled location, flight direction, and motion parameters. The target is assumed to be completely separated, so training data for multiple drones was not included. The reason that multiple drones in the TR are not considered is that the TFIs of multiple targets are very similar; a quadcopter has four blades, and their MDs fill considerable portions of the MDI; MDs of many blades of multiple drones may fill the entire MDI, so TFIs of multiple drones may become very similar, and therefore not distinguishable. In our simulations, classification results were seriously degraded due to multiple targets (results shown in Section IV).

Combinations of a single drone + a single bird were considered, assuming that a drone and a bird occur in the same range bin. Due to the difficulty in considering all combinations of the bird and the drone parameters, the training data were constructed in a random manner; i.e., the position of a drone was fixed with a random flight direction and motion parameters, then a bird with a random flight direction and random motion parameters was placed within the range resolution from the drone, then MD training images were constructed. In addition, the TR of a single bird was constructed by using a bird model that has uniformly-sampled positions, flight directions, and motion parameters.

The disadvantage of the second protocol is that classification may fail when multiple targets occur in a range bin because multiple targets are not considered in the TR. However, our simulations demonstrated that the P_c decrease caused by estimating the exact number of multiple drones was larger than the decrease caused by excluding multiple cases (results in Section IV). Also, modern high-resolution FMCW radars can effectively resolve different targets in a close range, so the effect of missing multiple targets is much smaller than the effect of classifying multiple drones.

C. THIRD PROTOCOL

The third protocol is to construct the TR considering a drone, a drone + a bird, two drones, two drones + a bird, two drones + two birds, a bird, and two birds (Fig. 8). This protocol considers two drones that can occur in a range bin, to the protocol can be effective in classifying up to two simultaneous drones; to consider the effect of birds, MDs of the single bird and the two birds are added to the TR. This assumption is valid because a high-resolution FMCW radar can separate multiple drones in the range domain without many drones overlapped; we assumed that at most two drones can overlap. In some situations, many drones can occur simultaneously, but we did not consider this rare case, and our simulations demonstrated that estimation of the number of multiple drones ≥ 3 decreased P_c considerably (results in Section IV). Likewise, the maximum number of overlapped birds was set to 2, assuming a bird of similar size to the drone.

The training data were constructed using MDIs obtained in similar observation geometries to those mentioned in the two protocols: TR for the single drone was constructed using uniformly-sampled position, flight direction, and motion parameters. For two drones, a random position was randomly selected and two drones with random directions and motion parameters were placed within the range resolution from the selected position. Similarly, for single drone + single bird and single drone + two birds, the position of the drone was first selected randomly with a random direction and random motion parameters, then the bird was placed within the range resolution from the drone with the random direction and the random motion parameters. Likewise, two drones + single bird and two drones + two birds were placed with random direction and the random motion parameters. A single bird was placed with uniformly-sampled position, flight direction, and motion parameters, and finally, two birds were placed as in the case of the two drones (Fig. 8).

IV. CLASSIFICATION RESULT

A. SIMULATION CONDITION

Simulations were conducted using X-band FMCW radar that had center frequency $= 9.6$ GHz and $T_{chirp} = 0.25$ ms, and observation was conducted for $T_{CPI} = 0.0385$ s. $B = 150$ MHz (1-m range resolution) was assumed. We assumed a normal-sized drone composed of four wings, each of which had four blades with the rotation frequency between 40 ($= f_{b,1}$) and 50 ($= f_{b,2}$) Hz. $a_b = 8$ cm and $b_b = 1.5$ cm were used for each blade (Fig. 1). For the bird, we assumed

TABLE 1. Simulation parameters.

Center frequency	10 GHz	b_b	15 cm
Chirp period	0.25 ms	$f_{w,1}$	4 Hz
T_{CPI}	0.0385 s	$f_{w,2}$	7 Hz
Bandwidth (B)	150 MHz	Range	300 - 1500 m
$f_{b,1}$	40 Hz	Altitude	10 – 1000 m
$f_{b,2}$	50 Hz	Azimuth angle	-45 - 45°
a_b	8 cm	Flight direction	±30°

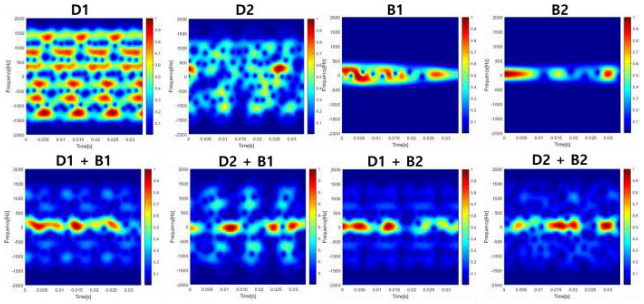

FIGURE 9. Examples of the MDIs of the combinations of the drone and the bird; D1 and D2 mean one and two drones, and B1 and B2 mean one and two birds.

wingspan = 60 cm, i.e., $a_w = b_w = 15$ cm with a flapping frequency f_w between $f_{w,1} = 4$ Hz and $f_{w,2} = 7$ Hz (Table 1).

TR of the single target was obtained by uniformly sampling the space and the parameter. The range was divided into 10 grids between 300 - 1500 m, the altitude was divided into 5 grids between 10 - 1000 m, and the azimuth angle for each range was divided into 5 grids between $-45 - 45°$. On each sampling point, the flight direction was sampled between $-\theta_t = -30°$ and $+\theta_t = 30°$ in increments $\Delta\theta_t = 1°$, and for each flight direction, the MDI was obtained by varying f_b and f_w in increments of 1 Hz. The function *findpeaks*() provided by MATLAB was used to clip the MD signal in the range bin containing the target. For the multiple targets, the position in the training space was randomly selected and the targets were randomly placed within the resolution cell (Table 1).

The MDI of the model looks very similar to that of the quadcopter in [23] (Fig. 9); due to the plate-shape of the blade, the blade flashes occur with a period that corresponds to the period of rotation (Fig. 12b in [23]). The low-frequency bird MD is similar to the measured bird except for the rigid-body MD that is caused by the uncompensated translational motion (Fig. 23 in [23]).

In the test, each target was flown in a random direction with a random parameter. In total, 2500 tests were conducted for each classification simulation. At a random position in the training space, a randomly-selected number of targets were flown in random directions with random motion parameters. Single-aspect classifications, i.e., classification using a single TFI, were first conducted to quantify the classification accuracy of each protocol (subsections IV.*B-D*), then majority

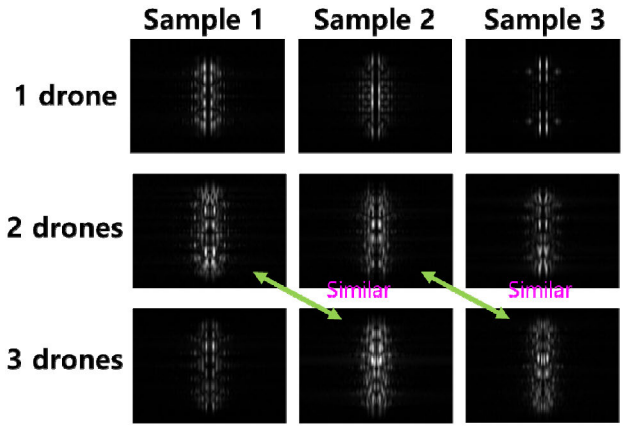

FIGURE 10. CVD samples for 1, 2, and 3 drones. CVDs of Drone 2 and 3 are similar CVDs because both have many blades; the normalized cross correlation was larger than 0.74.

TABLE 2. P_c [%] for cases of drones.

Cases	P_c	Cases	P_c
1 drone vs 1 bird	100	2 drones vs 3 drones	66.4
1 drone vs 2 drones	94.1	1 drone vs {2 or 3} drones	96.6
1 drone vs 3 drones	97.5	2 drones vs {1 or 3} drones	71.5

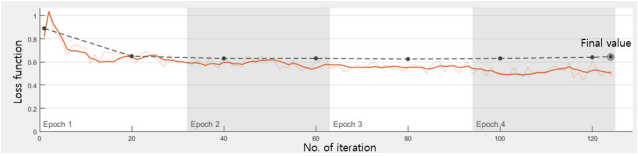

FIGURE 11. Variation of cost function vs iteration for classifying 2 and 3 drones (6000 training data). Due to the similarity of CVDs of 2 and 3 drones, the cost function did not converge.

vote was applied to further increase P_c (subsection IV.*E*) by using TFIs obtained for every 3 s.

B. SIMULATION RESULTS OF THE FIRST PROTOCOL

The first protocol does not consider overlapped multiple drones, so P_c may be affected considerably; therefore, a simulation was conducted to test the classification accuracy of CNN classifier for multiple drones, assuming SNR = 30 dB. Three CVDs for one drone were different from those for two drones and three drones (Fig. 10). However, due to the presence of 8 blades in the quadcopter and the limited space in TFI, the CVDs of two drones were very similar to those of three drones; the normalized correlation of similar figures were larger than 0.74 (formula defined in [22]).

P_c obtained by classifying each number of test targets were influenced by the shape of CVDs (Table 2). Because CVDs of a single target is very different from those of multiple targets, $P_c \geq 94.1$ % were obtained but the decreased P_c compared with single-drone classification = 100 % demonstrates that separation of multiple drones into a single drone in range domain is a very important factor for improving P_c. The cost function for classifying two and three drones did not converge, due to the similarity of their CVDs, so P_c was only

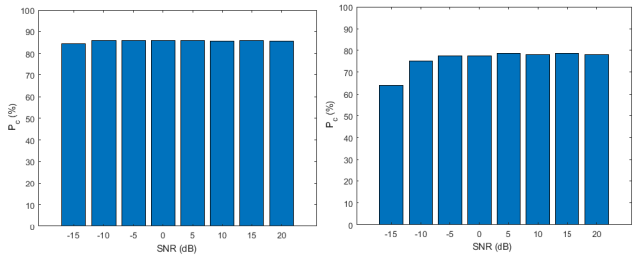

FIGURE 12. P_cs for the first (left) and the second (right) classifications of the first protocol. P_cs of the first classification degraded due to the overlap of the bird and the drone and the second classification degraded due to the similarity of TFIs of multiple drones.

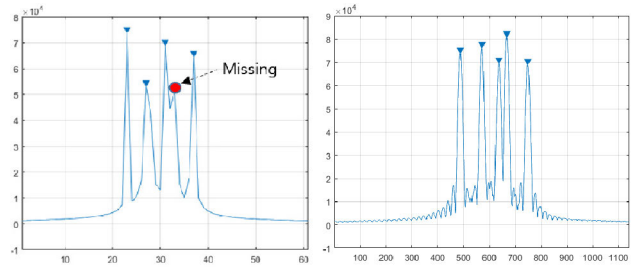

FIGURE 13. HRRPs before (left) and after (right) zero-padding to 1100 samples. A missed target is detected by zero-padding.

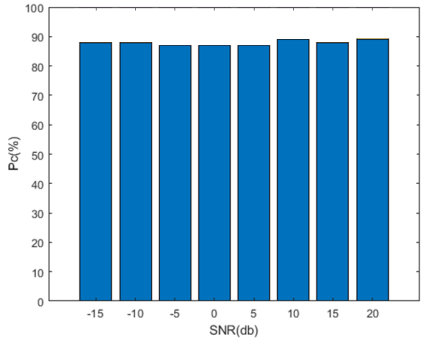

FIGURE 14. P_cs of HRRPs obtained by IFT of the zero-padding 64 samples to 1100 in the time-domain.

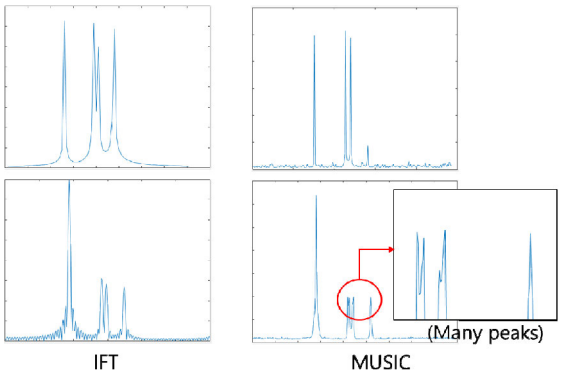

FIGURE 15. Comparison of HRRPs obtained by IFT and MUSIC.

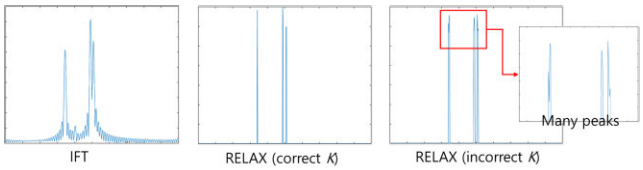

FIGURE 16. Comparison of HRRPs of three drones obtained by IFT and RELAX. Due to the unknown K, the RELAX algorithm failed to obtain the TFI of each drone, whereas the IFT algorithm successfully detected the peaks, and formed the TFI of each drone.

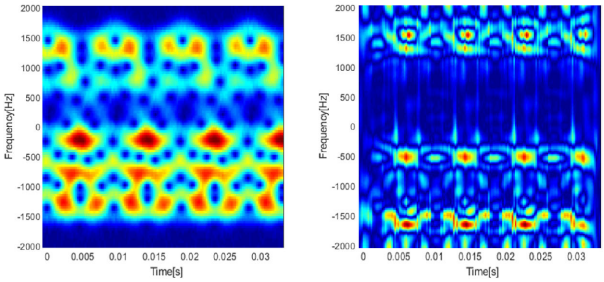

FIGURE 17. Comparison of STFT (left) and ZAM (right). Periodic MD of the blade is shown with a larger resolution in ZAM method than in STFT method.

66.4 %; this result demonstrates the difficulty in predicting the exact number of multiple drones (Fig. 11). For these reasons, P_c from the first step was reduced by $\sim$ 14 % and those in the second step was further reduced by $\sim$9 % at SNRs ≥ -10 dB, with the reduction caused by the occurrence of multiple drones in a range bin (Fig. 12).

The effect of zero-padding in time-domain before FT in the first step was also studied. The second step reduces P_c considerably, so simulations were conducted for the first step; the classification error was caused by overlap of drones, birds, or drone and birds. Zero-padding of 64 samples up to 1100 improved the separation of targets, so five peaks were detected even though one was missing before zero-padding (Fig. 13). However, overlapping of multiple targets was random and increased samples also increased the width of the target in HRRP, so P_c increased only by 3 - 4 % (Fig. 14).

The MUSIC and RELAX algorithms were both ineffective (Figs. 15, 16). Compared with HRRP by inverse FT (IFT), MUSIC provided RPs with a higher resolution but a single peak was divided into many peaks so targets could not be separated successfully in the range domain (Fig. 15). RELAX provided a better HRRP than MUSIC but failed to separate targets when the number K of scatterers was not correctly estimated; when K was larger than the number of scatterers, many peaks occurred, so targets were poorly separated and as a result, TFI of each target could not be formed (Fig. 16). This excessive number of peaks yielded low P_c which were $\sim$50 %, so these methods were not appropriate for multiple-target classification.

ZAM method was also tested for classifying two and three drones, and yielded P_c for various numbers of TR samples. The TFI of a quadcopter obtained using ZAM had higher resolution than that by STFT (Fig. 17). However, the time interval between large RCS values of blades was

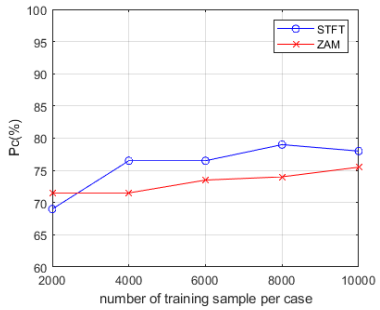

FIGURE 18. Comparison of P_cs obtained by STFT and ZAM for classifying two and three drones. Due to the similarity of TFIs of multiple drones, ZAM did not improve P_c.

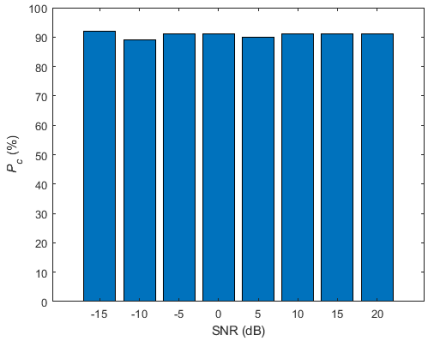

FIGURE 19. Classification results of the second protocol.

very short due to the high rotation speed of the blade, so most of the TFI of three quadcopters was filled, and the distinct characteristics for classification were lost. As a result, the cost function did not converge to 0 as in Fig. 11 so P_c obtained using ZAM were slightly lower than those of STFT, because of the cross-term interference among many scatterers (Fig. 18). This result supports our conclusion that classification of multiple drones in a range bin is a very difficult task (see Fig. 12).

Our conclusion on the first protocol is as follows: The most important factor for multiple target classification is the separation of the single target in the range domain so that the numbers and types of targets can be estimated with accuracy ∼100 %. Estimation of the number of drones considerably degrades P_c so this estimation should not be conducted in the first protocol. Zero-padding is helpful for separating targets by increasing the number of samples, but the two high-resolution methods are not adequate due to many peaks in a target. High resolution TF methods do not improve P_c, because fast rotation of many blades fills TFIs considerably, so TF images are similar. This conclusion provides a good direction for multiple drone-bird recognition.

C. SIMULATION RESULTS OF THE SECOND PROTOCOL

The second protocol is similar to the first step of the first protocol, because both assume that targets are separated in the range-domain, but the second protocol further assumes that a drone and a bird overlap in a range bin. Six thousand random

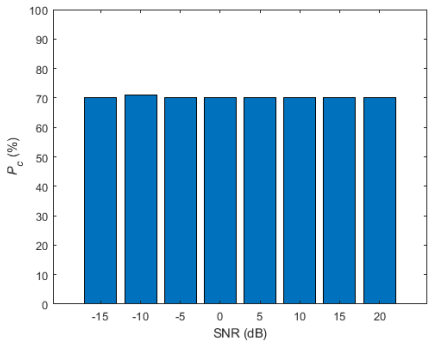

FIGURE 20. Classification results of the second protocol for multiple targets. P_c decreased considerably because the second protocol did not consider multiple drones and birds.

combinations were considered in the training database. Our main concern is to distinguish the drone from the bird, so a drone + a bird were considered as a drone while training the classifier.

The advantage of the second protocol is represented in the classification result; P_c of the second protocol was increased by 5 - 7 % compared with the result of the first step of the first protocol (Fig. 19). However, compared with the single-drone classification (Table 2), random occurrence of multiple drones, multiple birds, and combinations of birds and drones degraded P_c by 8 - 11 %. This result provides another direction for multiple drone classification in addition to that of the first protocol: The best way is to separate targets in the range domain, and the effect of the bird should be considered in the training database.

The disadvantage of the second protocol is that it does not consider multiple targets. To study the effect of multiple targets, we conducted another simulation. With the same training condition as in the first simulation, at least two targets were overlapped within a range resolution when the randomly selected number of targets ≥2; this condition caused more than two targets (drone-drone, drone-bird, bird-drone, bird-bird) to occur in a range bin. Compared with the result in Fig. 19, P_c decreased by 20 - 22 % (Fig. 20). This result demonstrates that the second protocol must consider possible combinations of drones and birds.

D. SIMULATION RESULTS OF THE THIRD PROTOCOL

The third protocol is similar to the second protocol, but considered overlaps of up to two drones and two birds. As in the second protocol, 6000 random cases for each combination were considered in the training database, and training was conducted considering the number of drones. The cases of a drone + a bird, and of two birds were considered as a drone. The cases of two drones + a bird and two birds were considered as two drones. Compared with the result of the second protocol, P_c of the third protocol were lower by 1 - 3 % than those of the second protocol because of adding TR of two drones (Fig. 21); adding TR of the two drones caused additional classification error in single drone classification due to the similar TFIs of one and two drones

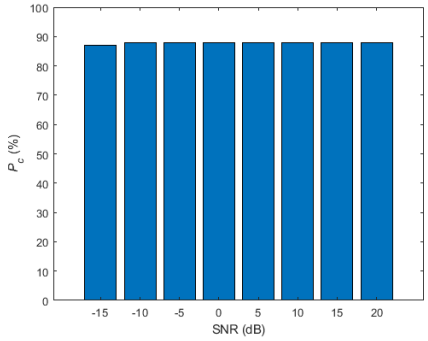

FIGURE 21. Classification results of the third protocol.

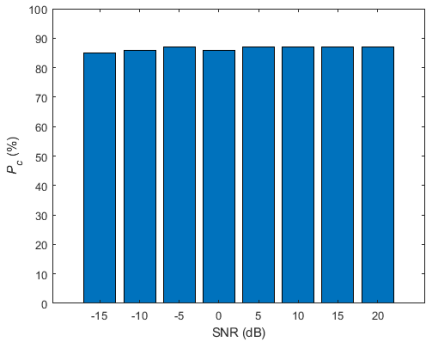

FIGURE 22. Classification results of the third protocol for multiple targets.

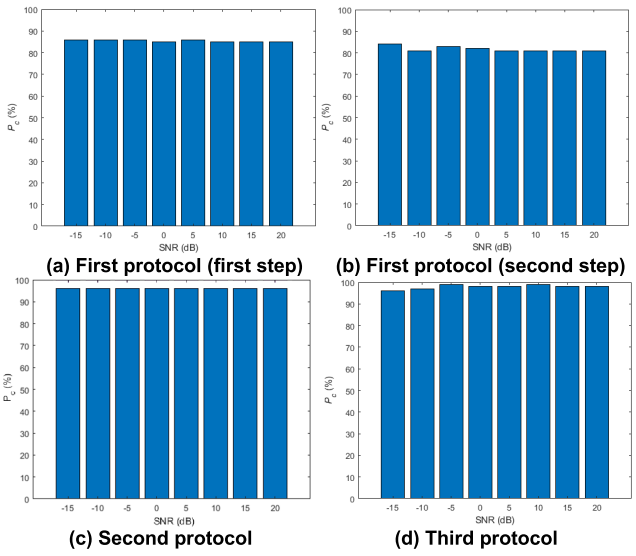

FIGURE 23. Multi-aspect classification results ($K = 5$).

(1 vs 2 drones in Table 2). In addition, the small decrease of P_c demonstrates that addition of two birds in TR did not affect the classification result considerably.

Comparison of the third protocol with the second protocol for the multiple target cases demonstrates the effectiveness of the third protocol. P_c of the third protocol decreased only by 1 - 3 % (Fig. 22), which is much smaller than decrease of ∼22 % caused by the second protocol. The decrease was

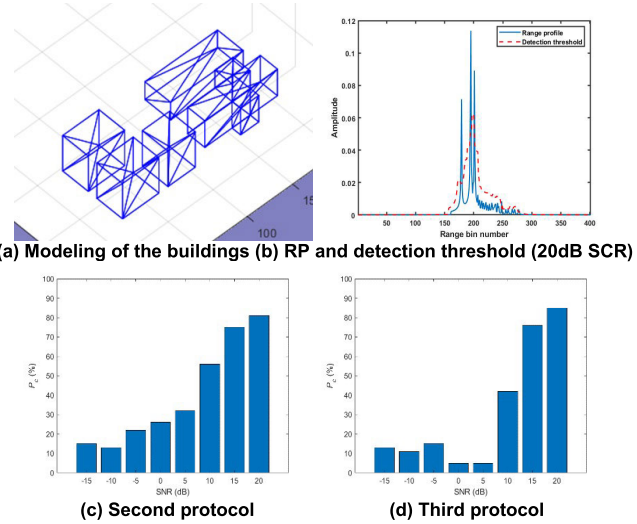

FIGURE 24. Classification results in clutter environment.

small because most of the cases were included in the TR and the cases of drones ≥3 and birds ≥3 were very rare. Therefore, our conclusion is as follows: even though best way to classify multiple targets is to separate them in the range domain (subsections IV.*B* and *C*), random combinations of two targets in the training database are required to cope with simultaneous occurrence of them.

E. SIMULATION RESULTS OF THE MULTI-ASPECT CLASSIFICATION

The accuracies of the protocol were compared using the majority vote introduced in (23). Five targets were randomly selected and $N_T = 5$ TFIs sampled at 3 s were used for classification according to the rule of majority vote (Fig. 23). For the first protocol, P_c increased by approximately 1 - 6 % compared with the single-aspect classification, as a result of the increased number of TFIs for SNR ≥ -10 dB. Simultaneous targets occurred frequently, so the improvement was as large as expected. P_c of the second protocol increased by 5 - 6 % and those of the third protocol increased by 10 - 12 %; these results demonstrate that the third protocol is the most adequate for multi-aspect classification. The third protocol includes most combinations of targets, so a target that is incorrectly classified by a TFI at a certain time can be correctly classified by other TFIs at different times. The result of multi-aspect classification may be dependent N_T and the sampling interval of TFIs, so further study to improve the classification accuracy must be conducted.

F. EVALUATION OF PROTOCOLS 2 AND 3 IN CLUTTER ENVIRONMENT

P_cs in Figs 12, 14, and 19 - 23 were obtained in clutter-free environments, however, the radar signal can be contaminated by clutter. In this subsection, we tested the second and third protocols by using the clutter signal of a building model

computed using physical optics (Fig. 24a). Using the center frequency and the bandwidth (Table 1), the radar signal was calculated at a random observation angle in increments of 1 MHz (unambiguous range = 150 m) and the calculated signals were transformed to an RP by inverse FT. Then, for a given clutter-to-signal ratio (SCR), RPs of the building model were adjusted and added to RPs of the target; to consider the random position, targets were positioned at random positions within the RP of the building. The other parameters were the same as in Fig. 19 and 21.

Peaks of the target in RPs were detected by applying the method that uses singular value decomposition [24], [25] and the ordered statics constant false alarm rate detector (OS-CFAR) [26]; clutter was removed by selecting the largest singular value and its vector, then OS-CFAR was applied to detect the target in the clutter-removed RP (Fig. 24b). Classification results demonstrate that SCR $\geq$ 15 dB is required for both methods (Fig. 24c and d). Compared with the result in Figs 19 and 21, P_c decrease was up to 12 % for SCR $\geq$ 15 dB; this reduction demonstrates that a poorly-detected target can degrade the accuracy considerably. This result can vary depending on the type of clutter; further research on this effect is required.

V. CONCLUSION

In this paper, we proposed three protocols to classify multiple drones and birds by using TFIs, and analyzed the accuracy of the protocols in various conditions. The classification results of the first protocol indicated that the most important factor for multi-target classification is to separate the target in the range domain; success at this task yielded $P_c \approx 100$ %, because the TR of the single target can be used. Estimation of the exact number of drones decreased P_c significantly because completely-filled TFIs of multiple drones were very similar. The second protocol that assumes drones are completely separated and that a bird can overlap with a drone; this protocol increased P_c by 5 - 7 % compared with the first step of the first protocol but was vulnerable to multiple targets within the resolution cell. Finally, the third protocol that considers the combination of two drones and a bird was the most adequate; $\geq$3 drones and $\geq$3 birds occurred very rarely, so P_c degraded only by 1 - 3 % compared with the second protocol. Multi-aspect classification using the rule of majority vote improved P_cs of the three protocols but the amount of P_c improvement for the third was much higher than that of the other two protocols because the third protocol included the possible combination of targets.

Real MDIs of multiple drones and birds are difficult to obtain, so classification results shown in this paper were obtained using simulated data, assuming the specifications of the radar that we are currently developing. For this reason, further study should consider measured data that include the effects of real-world interference such as noise, clutter, antenna beam pattern, and multi-path reflection. In addition, P_c should be analyzed using various real classification scenarios of multiple targets. We are currently conducting experiments to analyze the MD signal of real flying drones and birds, and multiple target classification will be conducted based on the measured data.

REFERENCES

[1] P. Tait, *Introduction to Radar Target Recognition*. Edison, NJ, USA: IET, 2005.

[2] S.-H. Park, M.-G. Joo, and K.-T. Kim, "Construction of ISAR training database for automatic target recognition," *J. Electromagn. Waves Appl.*, vol. 25, nos. 11–12, pp. 1493–1503, Jan. 2011.

[3] S.-K. Han, H.-T. Kim, S.-H. Park, and K.-T. Kim, "Efficient radar target recognition using a combination of range profile and time-frequency analysis," *Prog. Electromagn. Res.*, vol. 108, pp. 131–140, 2010.

[4] V. C. Chen, F. Li, S.-S. Ho, and H. Wechsler, "Micro-Doppler effect in radar: Phenomenon, model, and simulation study," *IEEE Trans. Aerosp. Electron. Syst.*, vol. 42, no. 1, pp. 2–21, Jan. 2006.

[5] T. Thayaparan, S. Abrol, E. Riseborough, L. Stankovic, D. Lamothe, and G. Duff, "Analysis of radar micro-Doppler signatures from experimental helicopter and human data," *IET Radar, Sonar Navigat.*, vol. 1, no. 4, pp. 289–299, Aug. 2007.

[6] J.-H. Jung, U. Lee, S.-H. Kim, and S.-H. Park, "Micro-Doppler analysis of Korean offshore wind turbine on the L-band radar," *Prog. Electromagn. Res.*, vol. 143, pp. 87–104, 2013.

[7] J.-H. Jung, K.-H. Kim, S.-H. Kim, and S.-H. Park, "Micro-Doppler extraction and analysis of the ballistic missile using RDA based on the real flight scenario," *Prog. Electromagn. Res. M*, vol. 37, pp. 83–93, 2014.

[8] L. Liu, D. McLernon, M. Ghogho, W. Hu, and J. Huang, "Ballistic missile detection via micro-Doppler frequency estimation from radar return," *Digit. Signal Process.*, vol. 22, no. 1, pp. 87–95, Jan. 2012.

[9] K. Chen, Y. Li, and X. Xu, "Rotating target classification base on micro-Doppler features using a modified adaptive boosting algorithm," in *Proc. Int. Conf. Comput., Commun., Syst. (ICCCS)*, Nov. 2015, pp. 236–240.

[10] S. Björklund, "Target detection and classification of small drones by boosting on radar micro-Doppler," in *Proc. 15th Eur. Radar Conf. (EuRAD)*, Sep. 2018, pp. 182–185.

[11] S. Björklund, H. Petersson, and G. Hendeby, "Features for micro-Doppler based activity classification," *IET Radar Sonar Navigat.*, vol. 9, no. 9, pp. 1181–1187, Dec. 2015.

[12] R. I. A. Harmanny, J. J. M. de Wit, and G. Premel-Cabic, "Radar micro-Doppler mini-UAV classification using spectrograms and cepstrograms," *Int. J. Microw. Wireless Technol.*, vol. 7, nos. 3–4, pp. 469–477, Jun. 2015.

[13] P. Molchanov, R. I. A. Harmanny, J. J. M. de Wit, K. Egiazarian, and J. Astola, "Classification of small UAVs and birds by micro-Doppler signatures," *Int. J. Microw. Wireless Technol.*, vol. 6, nos. 3–4, pp. 435–444, Jun. 2014.

[14] B. K. Kim, H.-S. Kang, and S.-O. Park, "Drone classification using convolutional neural networks with merged Doppler images," *IEEE Geosci. Remote Sens. Lett.*, vol. 14, no. 1, pp. 38–42, Jan. 2017.

[15] K. T. Kim, D. K. Seo, and H. T. Kim, "Efficient radar target recognition using the MUSIC algorithm and invariant features," *IEEE Trans. Antennas Propag.*, vol. 50, no. 3, pp. 325–337, Mar. 2002.

[16] H.-H. Y. Lu, "Super-resolution of stepped frequecy radar based on RELAX algorithm," in *Proc. IET Int. Radar Conf.*, Apr. 2009, pp. 1–4.

[17] L. Stankovic, "Auto-term representation by the reduced interference distributions: A procedure for kernel design," *IEEE Trans. Signal Process.*, vol. 44, no. 6, pp. 1557–1563, Jun. 1996.

[18] S.-W. Yoon, S.-B. Kim, J.-H. Jung, S.-B. Cha, Y.-S. Baek, B.-T. Koo, I.-O. Choi, and S.-H. Park, "Efficient classification of birds and drones considering real observation scenarios using FMCW radar," *J. Electromagn. Eng. Sci.*, vol. 21, no. 4, pp. 270–281, Sep. 2021.

[19] B. R. Mahafza, *Radar Systems Analysis and Design Using MATLAB*. Boca Raton, FL, USA: CRC Press, 2000.

[20] S. Qian and D. Chen, *Joint Time-Frequency Analysis: Methods and Applications*. Upper Saddle River, NJ, USA: Prentice-Hall, 1996.

[21] Y. Kim and T. Moon, "Human detection and activity classification based on micro-Doppler signatures using deep convolutional neural networks," *IEEE Geosci. Remote Sens. Lett.*, vol. 13, no. 1, pp. 8–12, Jan. 2016.

[22] R. O. Duda, P. E. Hart, and D. G. Stork, *Pattern Classification*. Hoboken, NJ, USA: Wiley, 2001.

[23] K.-B. Kang, J.-H. Choi, B.-L. Cho, J.-S. Lee, and K.-T. Kim, "Analysis of micro-Doppler signatures of small UAVs based on Doppler spectrum," *IEEE Trans. Aerosp. Electron. Syst.*, vol. 57, no. 5, pp. 3252–3267, Oct. 2021.

[24] A. Nezirovic, A. G. Yarovoy, and L. P. Ligthart, "Signal processing for improved detection of trapped victims using UWB radar," *IEEE Trans. Geosci. Remote Sens.*, vol. 48, no. 4, pp. 2005–2014, Apr. 2010.
[25] J. E. Kim, "Analysis of heavy radar clutter," Ph.D. dissertation, Dept. Elect. Eng., POSTECH, Pohang, South Korea, 2020.
[26] J.-H. Choi, K.-B. Kang, S.-G. Sun, J.-S. Lee, B.-L. Cho, and K.-T. Kim, "Efficient detection of small unmanned aerial vehicles in cluttered environment," *J. Korean Inst. Electromagn. Eng. Sci.*, vol. 30, no. 5, pp. 389–398, May 2019.

SEWON YOON received the B.S. and M.S. degrees in electronic engineering from Pukyong National University, Busan, South Korea, in 2017 and 2019, respectively, where he is currently pursuing the Ph.D. degree in electronic engineering. His research interests include the areas of radar target imaging and recognition, radar signal processing, target motion compensation, pattern recognition using artificial intelligence, and RCS prediction.

SOOBUM KIM received the B.S. and Ph.D. degrees in electronics engineering from the Pohang University of Science and Technology (POSTECH), Pohang, South Korea, in 1997 and 2002, respectively. He was with LIG Nex1, ISR Research Center, Electronics and Telecommunications Research Institute (ETRI), and Digitron Company Ltd., as a Senior Member of Research Staff, from 2003 to 2014. Since 2015, he has been the CEO of Radisys Corporation Ltd., Daegu, South Korea. His research interests include the system design and signal processing of radar and SAR systems.

JOOHO JUNG received the B.S. degree from the Korea Air Force Academy, Cheongju, South Korea, in 1991, and the M.S. and Ph.D. degrees in electronic engineering from POSTECH, in 1998 and 2007, respectively. From 2008 to 2012, he was a Lieutenant Colonel in-charge of planning national defense research and development in Defense Acquisition Program Administration, Seoul, South Korea. From 2012 to 2018, he was the Director of the Defense Research and Development (R&D) Strategy Center, POSTECH, and the Unmanned Safety Robot Center, Korea Advanced Institute of Science and Technology, and the Fusion Center for Security and Defense R&D, POSTECH. In 2020, he joined the Electromagnetic Technology Research Center, where he is currently the Director. His research interests includea radar target recognition, radar signal processing, and electromagnetic analysis on the wind farm by various military radars.

SANGBIN CHA received the B.S. and M.S. degrees in electronic engineering from Pukyong National University, Busan, South Korea, in 2017 and 2019, respectively, where he is currently pursuing the Ph.D. degree in electronic engineering. His research interests include the areas of radar target imaging and recognition, radar signal processing, target motion compensation, pattern recognition using artificial intelligence, RCS prediction, and electromagnetic analysis of the windfarm.

YOUNGSEOK BAEK received the B.S. and M.S. degrees in electronic engineering from Hanyang University, Seoul, South Korea, in 1985 and 1987, respectively. In 1989, he joined the Electronics and Telecommunications Research Institute (ETRI), Daejeon, South Korea, where he is currently a Senior Engineer. His research interests include CAD in semiconductor, digital design and verification methodology, wireless communication, face recognition, and radar signal processing.

BONTAE KOO received the M.S. degree in electrical engineering from Korea University, Seoul, Republic of Korea, in 1991. In 1991, he was with the System Semiconductor Division, Hyundai Electronics Company, Ichon, South Korea, where he was involved in the chip design of video codec and DVB modem. From 1993 to 1995, he was with HEA, Sanjose, USA, where he was responsible for the design of MPEG2 video codec chip. From 1996 to 1997, he was with TVCOM, Sandiago, USA. Developing the design of DVB modem chip. In 1998, he joined the System Semiconductor Laboratory, Dongbu Electronics, as the Team Leader, and he focused on the methodology of semiconductor chip design. In 1999, he joined the Application SoC Team, ETRI, where he was the Team Leader. His research interests include the chip design of MPEG4 video, T-DMB receiver, LTE femtocell modem, and DSP processor. In 2016, he joined the RF Research Group, ETRI, where he is currently the Project Leader. His research interest includes millimeter-wave AI radars.

INOH CHOI received the B.S. and M.S. degrees in electronic engineering from Pukyong National University, Busan, South Korea, in 2012 and 2014, respectively, and the Ph.D. degree from the Pohang University of Science and Technology (POSTECH), in 2020. In 2020, he joined the Agency for Defense Development as a Senior Researcher. In 2021, he joined the Department of Electronics and Communications Engineering, Korea Maritime and Ocean University, where he is currently an Assistant Professor. He was a recipient of the Best Paper Award from the Korea Institute of Electromagnetic Engineering and Science (KIEES). His current research interests include micro-Doppler analysis, radar signal processing, automotive target recognition, and calibration of polarimetric SAR.

SANGHONG PARK received the B.S., M.S., and Ph.D. degrees in electronic engineering from the Pohang University of Science and Technology (POSTECH), Pohang, South Korea, in 2004, 2007, and 2010, respectively. In 2010, he was a Brain Korea 21 Postdoctoral Fellow with the Electromagnetic Technology Laboratory, POSTECH. In 2010, he joined as a Faculty Member of the Department of Electronics Engineering, Pukyong National University, Busan, South Korea, where he is currently an Associate Professor. His research interests include radar target imaging and recognition, radar signal processing, target motion compensation, and radar cross section prediction.